# Roles of the matrix and of the primary carbides in the general high temperature oxidation behaviour of cobalt-based superalloys. Part 2: the Co(10Ni,30Cr) matrix with chromium carbides

Albert Leroy[1], Alexandre Navet[1], Thierry Schweitzer[2,3], Lionel Aranda[2,3], Patrice Berthod[2,3]*

[1]Lycée Henri Loritz, 29 rue des Jardiniers, 54000 Nancy, (FRANCE)
[2]University of Lorraine, Faculty of Sciences and Technologies, (FRANCE)
[3]Institut Jean Lamour (UMR 7198), Team 206 "Surface and Interface, Chemical Reactivity of Materials"
B.P. 70239, 54506 Vandoeuvre-lès-Nancy, (FRANCE)
E-mail: Patrice.Berthod@univ-lorraine.fr

## ABSTRACT

Most of the cast cobalt-based superalloys contain interdendritic carbides to strengthened them against mechanical solicitations at high temperature. Among the most common carbides used in this field there are the chromium carbides the formation of which does not necessitate new carbide-former elemnts since chromium is always present for oxidation and corrosion resistance purpose. Such carbides may influence the general oxidation behaviour of the whole alloy. In order to specify their contribution a cobalt alloy containing 10 wt.Ni and 30 wt.%Cr as most of cobalt-based superalloys, and 0.5 wt.%C to obtain chromium carbides in the microstructure, was studied in oxidation for the whole same thermal cycle as applied to a Co-10Ni-30Cr ternary alloy preliminarily characterized in the first part of this study. Many parameters describing the oxidation during the heating, the isothermal stage and the cooling were compared between these two alloys. There was not systematically differences but it significantly appeared that the {chromium carbides}-containing alloy oxidized faster during the heating and the isothermal stage than the carbides-free one. In contrast, if oxide spallation occurred for the studied alloy as previously also observed for the ternary alloy, this phenomenon was delayed later as is to say to lower temperatures.

© 2015 Trade Science Inc. - INDIA

## INTRODUCTION

The cast cobalt-based superalloys[1-3] represent an important family of refractory alloys, complementary to the nickel-based ones in the way of no dependence on gamma prime phase. Indeed, even if they are generally not so creep-resistant at very high temperature as the nickel-based γ'-reinforced single crystals[4] they bring serious solutions to applications requiring the triple resistance at high temperature against mechanical solicitations, corrosion to aggressive molten substances[5-6] and high tempera-

*Full Paper*

ture oxidation[7-8].

Containing about 10 wt.%Ni for stabilizing their austenitic matrix at all temperatures and 20 to 30 wt.% Cr – high chromium contents allowed by the absence of aluminium – these alloys present good mechanical resistance between room temperature and rather high temperature thanks to their intrinsically strong matrix as well as good resistance against the high temperature chemical attacks thanks to their chromia-forming behaviour. Furthermore these two properties may be improved by the presence of carbon which promotes the formation, with a small part of the 30 wt.%Cr, of chromium carbides. Indeed, at not too elevated temperature authorizing the persistence of these carbides, the interdendritic ones, primary precipitated during solidification or secondary precipitated during specific multi-stage heat-treatment, help respectively the interdendritic cohesion and the obstruction of dislocation slip, and the Cr supplying of the oxidation front. Other benefits of the presence of such carbides, thanks to their high hardness (1336 $Hv_{50g}$ for the $Cr_7C_3$, 1350 $Hv_{50g}$ for the $Cr_3C_2$ and 1650 $Hv_{50g}$ for the $Cr_{23}C_6$)[9], may be also an increase in wear resistance[10-13], notably in case of high volume fractions of such carbides.

The interdendritic chromium carbides emerge on machined surfaces and they offer local high concentration of the highly oxidable element chromium, by comparison with the surrounding matrix. It is thus clear that they play a particular role during the heating in oxidant gases. During isothermal oxidation the chromium carbides generally dissolve over an increasing depth (this leading to the development of the carbide-free zone. A first consequence of this is an efficient supplying of the oxidation front in chromium which may favour the maintenance of a chromia-forming behaviour which is good for the resistance of the alloy in isothermal oxidation. A part of these interdendritic carbides may also be oxidized on place, with as result the existence of local oxidation penetration which can be beneficial for the adherence of the external oxide scales during the cooling.

The purpose of this second part of the study is to specify the general high temperature oxidation of a cobalt-based alloy containing interdendritic chromium carbides, to compare its behaviour to the ones obtained in the first part[14] of this work concerning an alloy simulating the matrix of the present alloy, in order to finally precise the role of the chromium carbides on the oxidation start during the heating, the isothermal oxidation rate during the isothermal oxidation and on the scale spallation during the cooling.

## EXPERIMENTAL

The Co-10Ni-30Cr-0.5C (all contents being in wt.%) previously used in two recent works[15,16] to study the effect of water vapour on the high temperature oxidation of cobalt-based alloys in a furnace, was here considered again (microstructure reminded in Figure 1: dendritic matrix in pale grey and interdendritic chromium carbides in dark). The not used parts were machined, to obtain three parallelepipeds of about 3mm × 7mm × 7 mm, which were ground with SiC papers of grade 1200. The edges and corners were smoothed. The oxidation tests were realized in dry synthetic air (80%$N_2$-20%$O_2$) using a SETARAM TGA92 92-16.18 thermobalance. The heating was realized at +20K min⁻¹, the isothermal stage at 1000, 1100 or 1200°C during 40 hours, and the cooling rate at -5K min⁻¹.

The mass variations were recorded every 12.2 (test at 1000°C), 12.3 (test at 1100°C) or 12.4 (test at 1200°C) seconds. The mass gain files were corrected from the air buoyancy variations and plotted
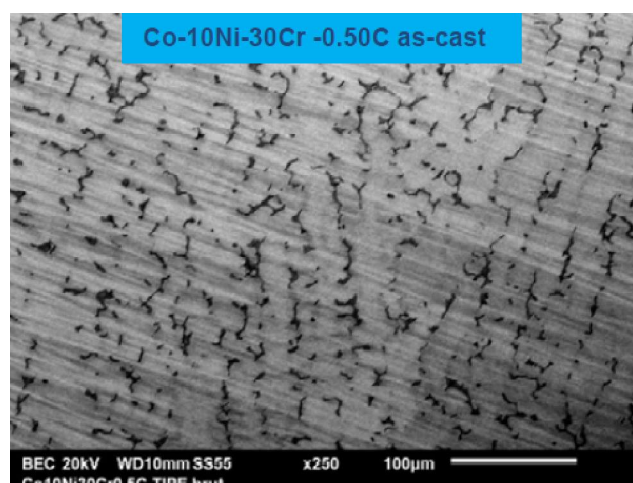


**Figure 1: SEM/BSE micrograph illustrating the as-cast microstructure of the studied alloy**

as mass gain versus temperature and exploited to specify the following characteristics:

**Heating**

- temperature at which the mass gain is significant enough to be detected by the micro-balance,
- eventual determination of the activation energy (if linear part in the curve describing the instantaneous linear mass gain rate variation with temperature, plotted according to the Arrhenius scheme),
- total mass gain achieved during the whole heating between the start of oxidation and the beginning of the isothermal stage),
- final linear mass gain rate when temperature reaches the isothermal stage one

**Isothermal stage**

- global shape of the mass gain curve when plotted versus time (parabolic or not, jumps or not),
- total mass gain exclusively achieved during the isothermal stage.

**Cooling**

- Temperature at which the mass variation accelerates or becomes irregular (start of scale spallation),
- final mass variation.

## RESULTS AND DISCUSSION

**Oxidation during heating**

The heating parts of the mass gain curves plotted versus temperature are presented together in Figure 2. It appears first that the common parts of the 1000°C-curve, the 1100°C-curve and the 1200°C curve are almost superposed. These three curves show that the mass gain by oxidation during the heating has become high enough to be detected by the used thermo-balance at a temperature which presents a rather bad reproducibility since the three values are spread over 800 - 875°C TABLE 1.

Over these temperatures of oxidation start the instantaneous linear kinetic constant increases more and more rapidly when temperature increases during the heating, this letting thinking to an exponential
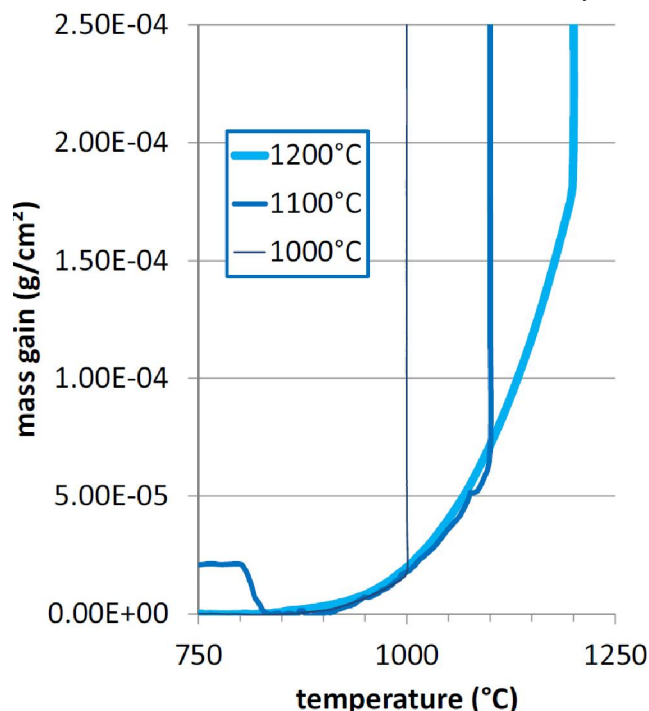


Figure 2 : Enlarged view of the mass gain curves recorded during heating until reaching 1000, 1100 or 1200°C

TABLE 1 : Values of the temperatures at which the mass gain by oxidation during heating has become significantly high enough

| 1000°C-test | 1100°C-test | 1200°C-test | reproducibility |
|---|---|---|---|
| 858.87 | 875.67 | 808.16 | rather bad |

increase with temperature. The Arrhenius plot confirms this over the whole heating from oxidation start or only on the high temperature part of the heating, since the points' clouds are globally elongated along a straight line. The slope of the regression straight line led to the values of activation energies listed in the first line of TABLE 2. These values are of the usual order of magnitude (between 150 and 230 kJ $Mol^{-1}$).

The second line of TABLE 2 presents the values of the final value of $(d\Delta m/S)/dt$ when temperature reaches the stage temperature. This final value of $K_l$ effectively increases with temperature, showing that oxidation is, at the beginning of the isothermal stage, logically faster when the stabilized temperature is higher. The values of the mass gains achieved during the whole heating are displayed in the third line of TABLE 2. They are also logically higher for a
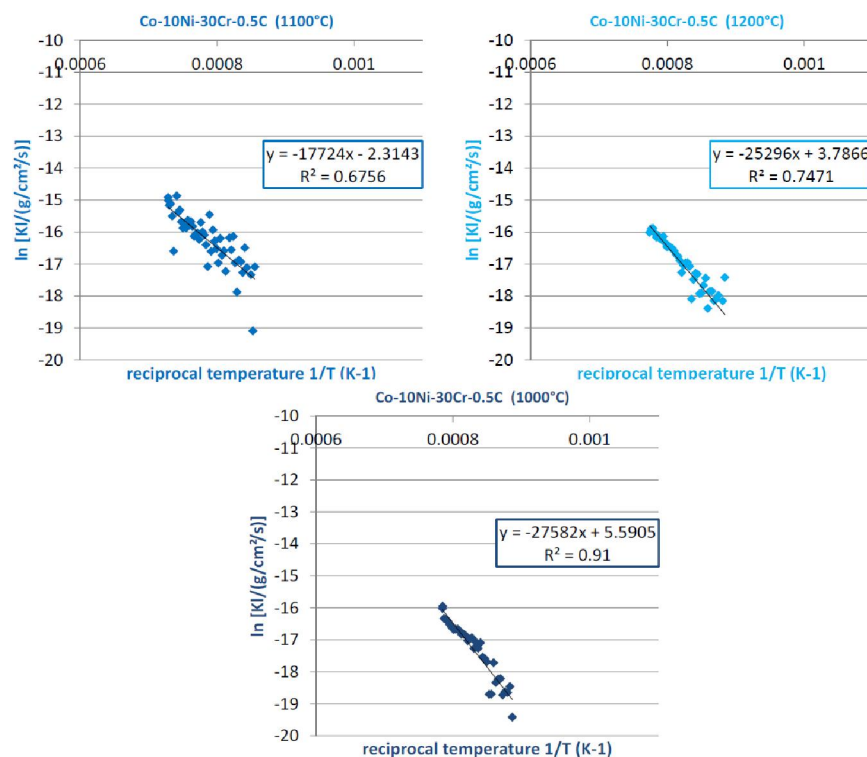
*Full Paper*



**Figure 3 : Arrhenius plot of the instantaneous linear oxidation constant over the whole heating (or only a part if the point's cloud is not straight elongated); values of the slope of the regression straight line for deducing the values of activation energies (displayed in TABLE 2)**

**TABLE 2 : Values of the activation energies characterizing the dependence on temperature of the linear oxidation constant $K_l$ issued from the successive values of $K_l$ noted during the heating (over the linear part of the Arrhenius plot); value of the $K_l$ value at the start of the isothermal stage**

| Q (J/Mol) issued from the $\ln((d\Delta m/S)/dt)$ plot versus 1/T(K) during heating | 1000°C-test | 1100°C-test | 1200°C-test |
|---|---|---|---|
| | 229317 | 147357 | 210311 |
| Final value of $K_l$ (end of cooling, beginning of the isothermal stage ($\times 10^{-8}$ g/cm²/s) | 10.45 | 25.40 | 48.13 |
| Mass gain at the end of heating (mg/cm²) | 0.019 | 0.069 | 0.205 |

higher temperature.

## Isothermal oxidation

When plotted as mass gain versus time the isothermal oxidation curves are globally parabolic. One can just notice that the curve obtained for 1000°C is initially affected by a small jump of mass gain just after the beginning of the isothermal stage, and that the curve obtained for 1100°C also present a visible mass gain jump near the middle of the isothermal stage. However, both of them are parabolic before and after the mass gain jumps. The curve obtained for 1200°C is more regular and thus wholly parabolic.

The mass gains achieved during the isothermal

stage are given for the three temperatures in the last column of TABLE 3. Logically the higher the stage temperature the higher the isothermal mass gain and, after addition of the mass gain achieved during heating (values reminded in the first results column of TABLE 3 again), the higher the total mass gain realized before cooling started (middle column).

## Phenomena at cooling

At the end of the isothermal stage the temperature decreased with a slow linear rate. At a given temperature the decrease in mass gain started then accelerated, the curve becoming more or less irregular: oxide scale spallation.

The temperatures at which this scale spallation

*Full Paper*

**TABLE 3 : Values of the temperatures at which the mass gain by oxidation during heating has become significantly high enough to be detected by the thermobalance**

| Oxidation test | Mass gain at the end of heating (mg/cm²); Proportion / heat.+isoth. (%) | Mass gain at the end of the isoth. stage (mg/cm²) (sum of ← and →) | Isothermal mass gain (mg/cm²); Proportion / heat.+isoth. (%) |
|---|---|---|---|
| 1200°C-test | 0.205 (3.79%) | 5.418 | 5.212 (96.21%) |
| 1100°C-test | 0.069 (2.33%) | 2.954 | 2.885 (97.67%) |
| 1000°C-test | 0.019 (1.34%) | 1.400 | 1.381 (98.66%) |

**TABLE 4 : Values of the temperatures at which spallation started during the cooling and final mass variation after return at room temperature**

| Oxidation test | Temperature of start of the cooling-induced scale spallation (°C) | Final mass variation at the end of the whole thermal cycle (mg/cm²) |
|---|---|---|
| 1200°C-test | 812.2 | -7.78 |
| 1100°C-test | 681.0 | -2.54 |
| 1000°C-test | 461.1 | -0.20 |

phenomenon occurred were red on the curves themselves, and the obtained values are given in the first results column of TABLE 4. One can see that the higher the isothermal stage temperature the higher the temperature of scale spallation start. The second results column gives the values of the final mass variations after return at ambient temperature. They are negative in the three cases, this demonstrating that the loss of oxide involving the loss of elements initially belonging to the alloy and the loss of oxygen atoms which had before induced a gain mass is finally higher than the gain mass initially given by the oxidation phenomenon.
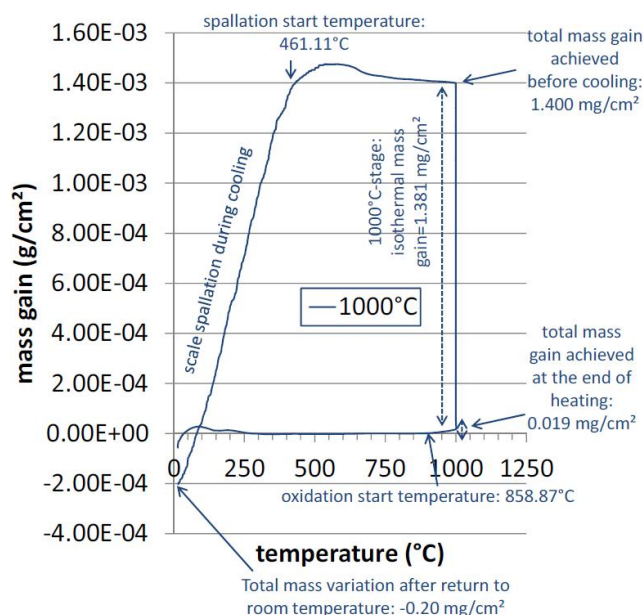
**Graphical summary**

The whole curves plotted as mass gain versus temperature are presented in Figure 4 for the 1000°C-test, Figure 5 for the 1100°C-test and in Figure 7 for the 1200°C test, with in each case the designation by arrows of the locations where the values of temperatures or of mass variations were red, as well as the obtained values already presented in the successive tables.

**General commentaries**

After having reproduced for this Co-10Ni-30Cr-0.5C alloy the same thermogravimetry experiments and the same analysis of the mass gain files some differences appear between the present {chromium

carbides}– containing alloy and the ternary alloy previously studied. First it seems that, with an average value of 847.59°C against 839.97°C, the oxidation start temperature at heating tends to be a little lower here than for the ternary alloy. However one has to be careful since the three values obtained for the three thermogravimetry tests in each cases were rather scattered, with variations higher than the difference existing between the two average values. As a matter of fact one must say that there is no sig-



**Figure 4 : The {mass gain versus temperature}-plot for the whole thermal cycle of the 1000°C-oxidation test**
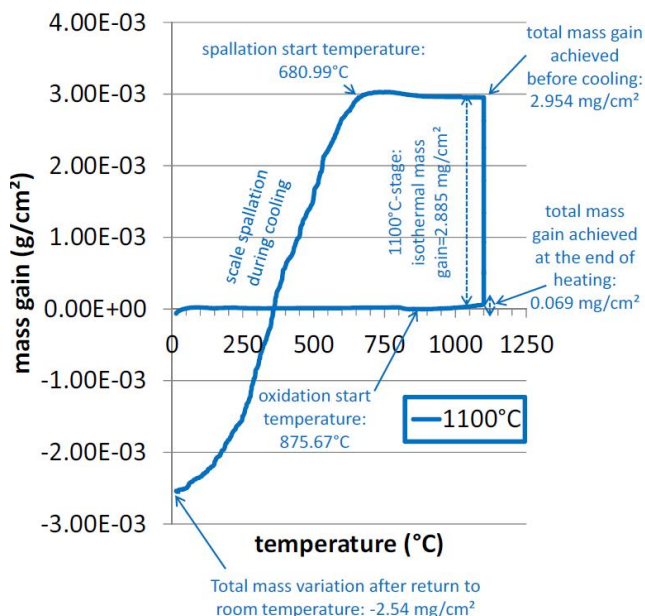
*Full Paper*



**Figure 5 : The {mass gain versus temperature}-plot for the whole thermal cycle of the 1100°C-oxidation test**



**Figure 6 : The {mass gain versus temperature}-plot for the whole thermal cycle of the 1200°C-oxidation test**

nificant difference between the two about this first parameter characterizing the oxidation at heating. Concerning the linear kinetic constant at the beginning of the isothermal stage there is no great difference and no systematic order between the two alloys for the three temperatures. In contrast it seems that the total mass gain achieved during the whole heating is systematically higher for the present quaternary alloy than for the ternary one: +52.6%, +34.8% and +26.3% more, for heating up to 1000°C, 1100°C and 1200°C respectively. During the isothermal stage the mass gain are again more important for the Co-10Ni-30Cr-0.5C alloy than for the Co-10Ni-30Cr one, with +66.0%, +26.0% and +17.9% more, for heating up to 1000°C, 1100°C and 1200°C respectively. In addition, one can notice that, in both cases, the relative difference decreases when the temperature increases. It is also interesting to see that the proportion of "heating" mass gain in the total "heating + isothermal" mass gain is systematically a little higher for the quaternary alloy than for the ternary one (with logically the inverse order for the proportion of "isothermal" mass gain).

Concerning the start of spallation and the consequences of this phenomenon on the final mass variation, the temperature of scale spallation start is systematically lower for the present carbides-containing alloy than for the carbide-free alloy which met
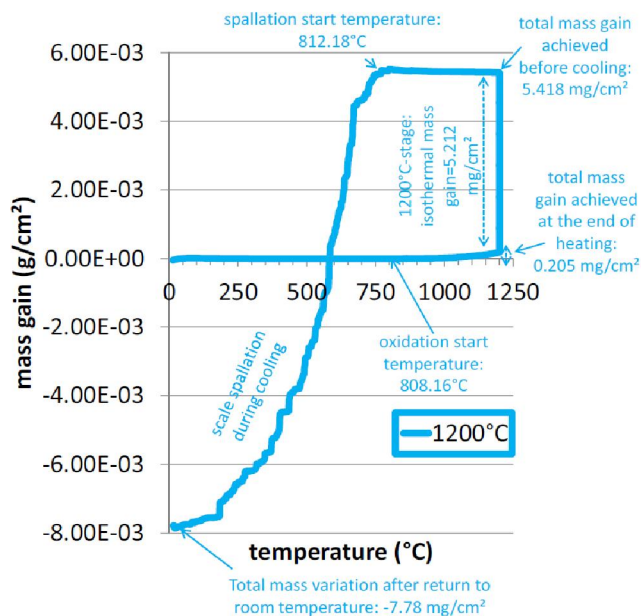
spallation start at higher temperatures, as is to say sooner during the cooling; indeed, by comparison with the ternary alloy, oxide spallation started here at two hundreds degrees lower, seventy degrees and one hundred degrees bellow (exactly -196°C, -72°C and -101°C), respectively for the cooling from 1000°C, 1100 and 1200°C. It seems that the presence of chromium carbides delays the spallation to lower temperatures. This results in final mass variations which are less important (negative in all cases but with absolute values higher for the ternary alloy than for the present carbide-containing one, but this is not really better for the present alloy since the previous mass gain by oxidation was higher and then the mass lost by spallation is not necessarily lower than for the ternary alloy.

**CONCLUSIONS**

Thus, the same thermal cycles applied in the same atmosphere led to small and no systematic differences for some parameters but to systematic and significant differences for other parameters. In the second case it was interestingly noticed that the presence of chromium carbides tended to speed up mass gain during the heating and thereafter during the isothermal stage, which is not favourable for a good behaviour in high temperature oxidation. In contrast,

*Full Paper*

despite that the mass gain by oxidation was higher for a given stage temperature – and consequently the scale thickness higher in the hypothesis of equivalent oxide volume masses and oxide porous states, spallation occurred later for the carbide-containing alloy than for the carbide-free one.

This work will be carried on, in a third last part, with the examination of the case of a tantalum-carbides containing alloy[17] the matrix of which is also comparable to same ternary alloy.

## REFERENCES

**[1]** C.T.Sims, W.C.Hagel; 'The superalloys', John Wiley & Sons, New York **(1972)**.

**[2]** A.M.Beltram; 'Superalloys II-High temperature materials for aerospace industry power', John Wiley, New York, 135 **(1987)**.

**[3]** E.F.Bradley; 'Superalloys: A Technical guide", ASM International, Metals Park, **(1988)**.

**[4]** M.J.Donachie, S.J.Donachie; 'Superalloys: A Technical Guide" (2nd Edition), ASM International, Materials Park, **(2002)**.

**[5]** J.Di Martino, C.Rapin, P.Berthod, R.Podor, P.Steinmetz; Corrosion Science, **46**, 1849 **(2004)**.

**[6]** J.Di Martino, C.Rapin, P.Berthod, R.Podor,

**[7]** P.Steinmetz; Corrosion Science, **46**, 1865 **(2004)**.

**[7]** P.Kofstad; 'High Temperature Corrosion', Elsevier applied science, London, **(1988)**.

**[8]** D.Young; High temperature oxidation and corrosion of metals, Elsevier, Amsterdam, **(2008)**.

**[9]** G.V.Samsonov; 'High-Temperature Materials – N°2: Properties Index', Plenum Press, New York **(1964)**.

**[10]** A.Klimpel, L.A.Dobrzanski, A.Lisiecki, D.Janicki; Journal of Materials Processing Technology, **1068**, 164-165 **(2005)**.

**[11]** Z.T.Wang, H.H.Chen; Mocaxue xuebao tribology, **25**, 203 **1068**.

**[12]** H.Han, S.Baba, H.Kitagawa, S. A.Suilik, K.Hasezaki, T.Kato, K.Arakawa, Y.Noda; Vacuum, **78**, 27 **(2005)**.

**[13]** D.Zhang, X.Zhang; Surface and Coating Technology, **190**, 212 **(2005)**.

**[14]** A.Navet, A.Leroy, T.Schweitzer, L.Aranda, P.Berthod; Materials Science: An Indian Journal, submitted.

**[15]** P.Berthod, L.Aranda, T.Schweitzer, A.Leroy, A.Navet; Materials Science: An Indian Journal, submitted.

**[16]** P.Berthod, L.Aranda, T.Schweitzer, A.Navet, A.Leroy; Materials Science: An Indian Journal, submitted.

**[17]** A.Navet, A.Leroy, T.Schweitzer, L.Aranda, P.Berthod; Materials Science: An Indian Journal, submitted.